Ultra-broadband chirp spread spectrum communication in the terahertz band

Sen, Priyangshu, Pandey, Honey, Jornet, Josep

Priyangshu Sen, Honey Pandey, Josep M. Jornet, "Ultra-broadband chirp spread spectrum communication in the terahertz band," Proc. SPIE 11390, Next-Generation Spectroscopic Technologies XIII, 113900G (19 May 2020); doi: 10.1117/12.2558914

SPIE.

Event: SPIE Defense + Commercial Sensing, 2020, Online Only, California, United States

Invited Paper

Ultra-broadband Chirp Spread Spectrum Communication in the Terahertz Band

Priyangshu Sen[1], Honey Pandey[2], and Josep M. Jornet[1]

[1]Department of Electrical and Computer Engineering, Northeastern University
Boston, MA, USA
[2]Department of Electrical Engineering, University at Buffalo, State University of New York
Buffalo, NY, USA

ABSTRACT

Terahertz (THz) band (0.1-10 THz) communication is envisioned as a key wireless technology to support faster and denser wireless networks. However, absorption by water vapor molecules splits the THz band into multiple transmission windows, each tens to hundreds of Gigahertz (GHz) wide. Because of the broadening of the absorption lines, the available bandwidth within each transmission window changes drastically with distance. As a result, a large portion of the bandwidth close to the absorption lines is considered not practical for communications or, in the best case, practical only for short-range applications. In this paper, chirp spread spectrum communication is proposed as a way to enable ultra-broadband communication links spanning across absorption lines in the THz band. More specifically, first, the performance of Chirp-Spread Binary Phase Shift Keying (CS-BPSK) is analytically derived and compared to that of Binary Chirp Spread Spectrum (BCSS) as well as non-spread Binary Phase Shift Keying (BPSK). Extensive numerical results based on an analytical channel model of the THz band are provided to illustrate the performance of the proposed scheme. Finally, experimental results above conducted in the first absorption-defined window above 1 THz are provided, validating the original hypothesis and highlighting the opportunities and challenges in communication across absorption lines at THz frequencies.

Keywords: Terahertz Communication; Ultra-broadband Modulations; Molecular Absorption; Spread Spectrum; Chirp; Experimental Results

1. INTRODUCTION

The demand for wireless data traffic has drastically increased due to the way today's society creates, shares, and consumes information. The need to provide wireless data connectivity anywhere and anytime leads to the generation of tens of exabytes of mobile data traffic per month with billions of mobile devices connected to the internet.[1] The need to provide faster wireless data rates to an ever-increasing number of wirelessly connected devices due to the boom in the Internet of Things (IoT) industries motivates the quest for untapped spectral resources. In this context, Terahertz band (0.1–10 THz) communication is envisioned as a key technology to satisfy the challenge of facilitating faster data rates in denser networks, in both traditional networking paradigms as well as novel nanoscale communication networks.[2–4]

For many years, the lack of compact and efficient signal sources, mixers, and detectors have limited the feasibility of long-range communications in the THz band. With many recent advancements in different THz device technologies that can operate at room temperature, the so-called THz band technological gap is finally closing. In the case of frequency up-converting electronic systems, high performance in terms of output power, noise figure, and efficiency has been demonstrated with III-V semiconductor technology.[5–7] In the case of frequency down-converting photo mixing systems, photodiodes are utilized to generate high power signal at THz

Further author information: (Corresponding Author: Priyangshu Sen)
Priyangshu Sen: E-mail: sen.pr@northeastern.edu
Honey Pandey: E-mail: honeypan@buffalo.edu
Josep M. Jornet: E-mail: jmjornet@northeastern.edu

Next-Generation Spectroscopic Technologies XIII, edited by Luisa T.M. Profeta,
Abul K. Azad, Steven M. Barnett, Proc. of SPIE Vol. 11390, 113900G · © 2020 SPIE
CCC code: 0277-786X/20/$21 · doi: 10.1117/12.2558914

frequencies.[8–10] Moreover, with the recent development of nanomaterial technology such as graphene, novel plasmonic transceivers and antennas have been demonstrated to intrinsically operate in the THz band.[11]

While the THz band provides unprecedentedly large bandwidth for wireless communication ranging from several tens of GHz up to a few THz,[12] the challenges introduced by very high propagation losses[13] at these frequencies remain. In addition to the spreading or free-space path loss, another key phenomenon affecting the propagation of THz-band signals is the absorption by water vapor molecules. The photon energy of THz signals (from 0.4 meV to 40 meV), while non-ionizing, triggers vibrational-rotational modes in gaseous molecules (primarily water vapor) that lead to sharp absorption lines across the THz band. For a communication distance below 1 m, the number of the gaseous molecules found along with the path is low, and the THz band can be considered as a single transmission window, several THz wide. This substantial bandwidth has motivated the use of very short pulse-based broadband modulations.[14] However, as the distance increases, molecular absorption becomes non-negligible, and the available bandwidth is split into multiple smaller transmission windows (each tens to hundreds of GHz wide). Furthermore, as the number of absorbing molecules increases, not only the absorption loss rises, but the absorption peaks become wider, affecting a larger bandwidth. The phenomenon is known as the broadening of the absorption lines.[13] Therefore, the bandwidth of each transmission window shrinks with the increasing transmission distance. As a consequence, different innovative modulation and waveform design techniques have been proposed for distance-dependent absorption-defined transmission windows.[15,16]

Despite these new modulation techniques, a large amount of bandwidth is wasted across the absorption lines depending on the operating frequency, distance and channel conditions (such as humidity, temperature and pressure). Additionally, the channel across the absorption peaks is highly frequency selective. In light of this, the Chirp Spread Spectrum (CSS) modulation appears as a suitable scheme to support robust communication in the THz band. Linear chirp signals have been used extensively in radar and sonar applications due to their correlation characteristics and robustness against doppler and multipath propagation delays.[17,18] In wireless communications, the use of a chirp signal was first proposed by Winkler in 1962.[19] Chirp Spread Spectrum has gained massive recognition in low power wireless communications as the IEEE 802.15.4a standard implements it as one of two possible physical layers.[20] For underwater communication, linear chirp based technology has been proposed for time/frequency synchronization, channel estimation, and wireless feedback communications.[21,22] Furthermore, to reduce the cross-correlation similarity, quasi-orthogonal chirps have been proposed for Multicarrier Chirp-Division Multiplexing (MCDM) in underwater networks.[23] However, linear chirp modulations cannot obtain negative cross-correlation coefficients. Due to this limitation, research groups have considered utilizing nonlinear chirps in forms of third-power function chirps and exponential chirps.[24] Though nonlinear chirps can obtain negative cross-correlation coefficients, increased system complications discourage their use for actual CSS based systems .[25] In the THz regime, application of chirp based technology is currently limited to the THz imaging and spectroscopy.[26,27]

In this paper, we investigate CSS schemes able to support multi-Gigabits-per-second (Gbps) communication links across absorption lines and, thus, maximize the utilization of the THz channel. More specifically, Chirp-Spread Binary Phase-Shift Keying (CS-BPSK) is proposed to establish wireless links over the absorption peaks, as a way to enable access to the frequencies that cannot be utilized for communications otherwise. Furthermore, we compare the performance of the proposed modulation scheme analytically and numerically with traditional Binary Chirp Spread Spectrum (BCSS) as well as non-spread Binary Phase Shift Keying (BPSK). The idea behind CS-BPSK is to obtain negative cross-correlation for a better Bit Error Rate (BER) performance and obtain a robust modulation scheme for communication across the absorption peak by exploiting its frequency spreading nature. Moreover, to validate our results, we conduct extensive experimental results utilizing the TeraNova testbed, a state of the art platform for THz communication.

The rest of this paper is organized as follows. In Section 2, we describe the peculiarities of the THz channel and motivation behind the work. In Section 3, we describe the proposed CS-BPSK modulation scheme and the fundamental differences when compared to BCSS. We analytically investigate the performance of the proposed scheme in terms of BER, and compare it with other traditional modulation schemes in Section 4. We provide experimental results in Section 5 and conclude the paper in Section 6.

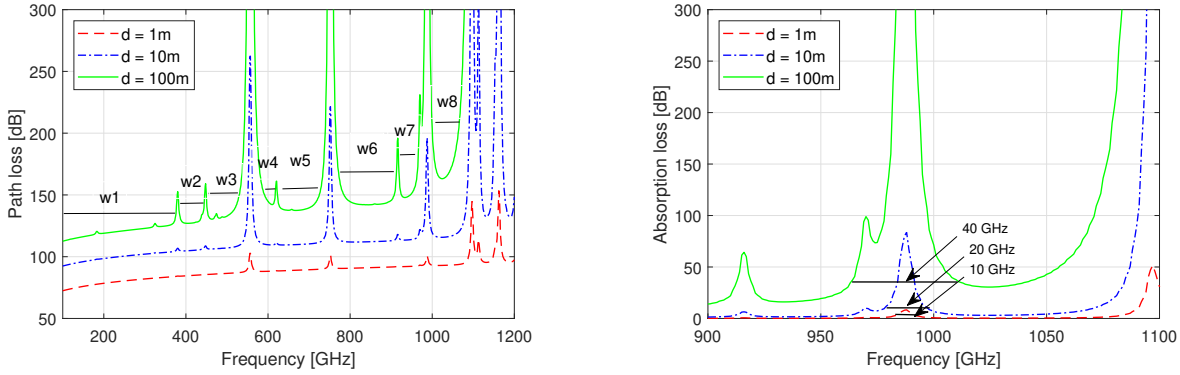

(a) Path loss

(b) Absorption loss at 988 GHz

Figure 1: Path loss (left) and absorption loss focused on 988 GHz (right) to demonstrate extent of absorption band with different distance

2. TERAHERTZ BAND CHANNEL MODEL

The path loss for line-of-sight (LoS) wireless communication links at THz-band frequencies is mainly determined by the spreading loss and the molecular absorption loss. Analytically, it is represented[13] by

$$PL_{LOS}(f,d) = \left(\frac{4\pi f d}{c}\right)^2 e^{k_{abs}(f)d}, \tag{1}$$

where f is the carrier frequency, d stands for communication distance, c denotes the speed of light in free space, and k_{abs} is the frequency-dependent absorption coefficient of the medium.

In Figure 1(a), the frequency-dependent path loss in dB is shown for transmission distances of 1 m, 10 m, and 100 m, for a standard atmosphere with 40% humidity. It is observed that molecular absorption from water vapor divides the available bandwidth into several transmission windows (w1, w2, w3, ... in Fig. 1). Moreover, with the increasing distance, the total number of interacting molecules increases, which not only increases the absorption loss but also leads to broadening of the absorption peaks. In other words, the bandwidth of the transmission windows shrinks as the length of the wireless link increases.

While there are modulation schemes that try to optimize bandwidth utilization without transmission over the absorption peaks;[15,16] ultimately tens of GHz of bandwidth remain underutilized depending on the distance and operating frequency. For instance, as shown in Figure 1(b), if the 988 GHz absorption line is considered, then 10 GHz, 20 GHz, and 40 GHz of bandwidth across it remain underutilized for a wireless link of 1 m, 10 m, and 100 m, respectively. Therefore, the high absorption loss and frequency selective nature of the absorption bands, i.e. the band across the absorption lines, motivates the use of CSS based communication systems.

3. CHIRP-SPREAD BINARY PHASE SHIFT KEYING

To maximize channel utilization while minimizing or, at least, upper-bounding the BER, we propose CS-BPSK for communication across the absorption peaks in the THz band. In this section, we mathematically describe this modulation scheme and illustrate the waveform structures.

The proposed CS-BPSK is partially related to the concept of CSS and consists in transmitting either an up-chirp (i.e., signal with increasing frequency sweep) or a down-chirp (i.e., signal with decreasing frequency sweep). The required phase shift is provided to modulate the symbol according to the bitstream. A symbol $s_m(t)$ is represented by

$$s_m(t) = \sqrt{\frac{2}{T_s}} \cos\left(2\pi f_0 t - \pi \mu_0 t^2 + \phi_m\right), 0 \le t \le T_s, \tag{2}$$

where T_s denotes the symbol duration and f_0 and μ_0 are the initial frequency and the frequency sweep rate, respectively. When we transmit an up-chirp signal, $f_0 = f_{min}$ and $\mu_0 = -\frac{B}{T_s}$ whereas for down-chirp signal

$f_0 = f_{max}$ and $\mu_0 = \frac{B}{T_s}$, where the bandwidth B of the chirp signal is the difference between the maximum and the minimum frequencies ($f_{max} - f_{min}$). ϕ_m refers to the phase of the m^{th} chirp waveform. For a binary scheme, $m \in (1, 2)$. Here, the value of f_0 and μ_0 is independent of the bits transmitted, whereas the phase, ϕ_m, is modulated according to the information bits. In our case, the up-chirp signal is utilized. The waveforms s_1 for bit "0" and s_2 for bit "1" are illustrated in Figure 2(a) and given by

$$s_1(t) = \sqrt{\frac{2}{T_s}} cos\left(2\pi f_{min} t + \pi \frac{B}{T_s} t^2\right), \tag{3}$$

$$s_2(t) = \sqrt{\frac{2}{T_s}} cos\left(2\pi f_{min} t + \pi \frac{B}{T_s} t^2 + \pi\right). \tag{4}$$

For comparison purposes, the mathematical description of the traditional BCSS is also provided. The BCSS with linear frequency sweep is given by[23]

$$s'_m(t) = \sqrt{\frac{2}{T_s}} cos\left(2\pi f_m t - \pi \mu_m t^2 + \phi_0\right), 0 \leq t \leq T_s, \tag{5}$$

where T_s is the symbol duration and ϕ_0 stands for the phase of the symbol. Unlike CS-BPSK, the initial frequency, f_m, consists of minimum frequency and maximum frequency of the IF band (i.e., $f_m = f_{min}$ and $f_m = f_{max}$, respectively) depending on the information bits transmitted. Therefore, the frequency sweep, μ_m, is comprise of $\mu_m = -\frac{B}{T_s}$ for up-chirp signal and $\mu_m = \frac{B}{T_s}$ for down-chirp signal. Here, the up-chirp signal is utilized to transmit bit "0", and the down-chirp signal is used to transmit bit "1", and the corresponding signals are given by s'_1 and s'_2, respectively, for the binary scheme. The corresponding waveforms are illustrated in Figure 2(b) and the symbols are written as

$$s'_1(t) = \sqrt{\frac{2}{T_s}} cos\left(2\pi f_{min} t + \pi \frac{B}{T_s} t^2\right), \tag{6}$$

$$s'_2(t) = \sqrt{\frac{2}{T_s}} cos\left(2\pi f_{max} t - \pi \frac{B}{T_s} t^2\right). \tag{7}$$

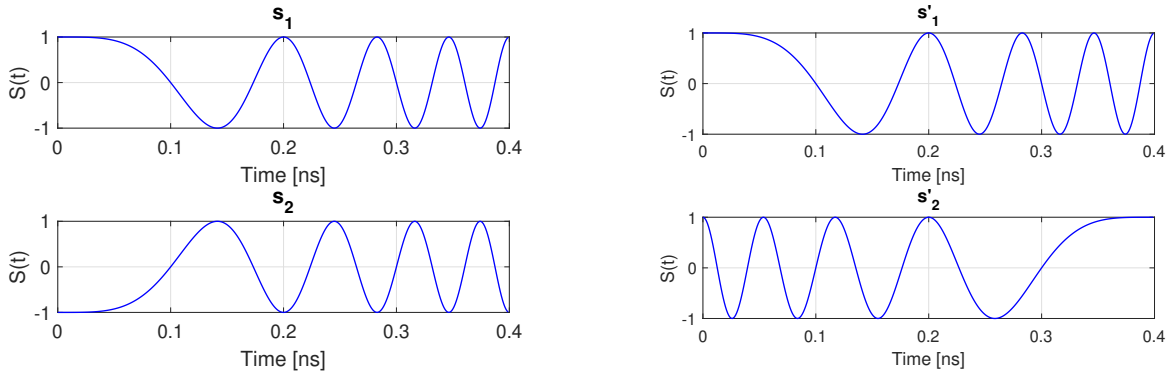

(a) CS-BPSK (b) BCSS

Figure 2: Waveform for CS-BPSK (left) and BCSS (right) with 20 GHz of bandwidth and 2.5 Gbps of data rate corresponding to information bit 0 and 1, which are represented by s_1 and s_2, respectively.

4. BIT ERROR RATE ANALYSIS

In this section, the performance in terms of BER of the proposed CS-BPSK scheme is investigated in the presence of Additive White Gaussian Noise (AWGN) for wireless communication across absorption bands. The probability

of error, P_e, for CSS schemes in a flat channel in the presence of AWGN is given by[23]

$$P_e = Q\left(\sqrt{\frac{E_b}{N_0}(1-\rho)}\right), \tag{8}$$

where ρ is the normalized cross-correlation coefficient between different modulated symbols, E_b stands for the energy per bit, and $\frac{N_0}{2}$ denotes the noise variance at the receiver. Mathematically, ρ is given by

$$\rho = \frac{1}{T_s}\int_0^{T_s} s_1(t)s_2(t)dt. \tag{9}$$

Depending on the cross-correlation between the signals, ρ takes a value between -1 to 1, i.e., $-1 \leq \rho \leq 1$. In the case of CS-BPSK, the phase shift between the frequency spread signals is π (Section 3). Consequently, the value of ρ is -1, similar to "not spread" BPSK. Thus, the probability of error is given by

$$P_e = Q\left(\sqrt{\frac{2E_b}{N_0}}\right). \tag{10}$$

For BCSS, the value of ρ depends on the time-bandwidth product and initial frequency, f_m, of the signals.[28] In Figure 3, the analytical probability of error in the flat channel is shown. Additionally, a simulated result (using Matlab) is provided comparing the BPSK, BCSS, and CS-BPSK modulation schemes. The analytical results match with simulated result closely, thus, validating our system design. It is observable that in the flat channel BPSK, CS-BPSK has the same probability of error and lower than BCSS.

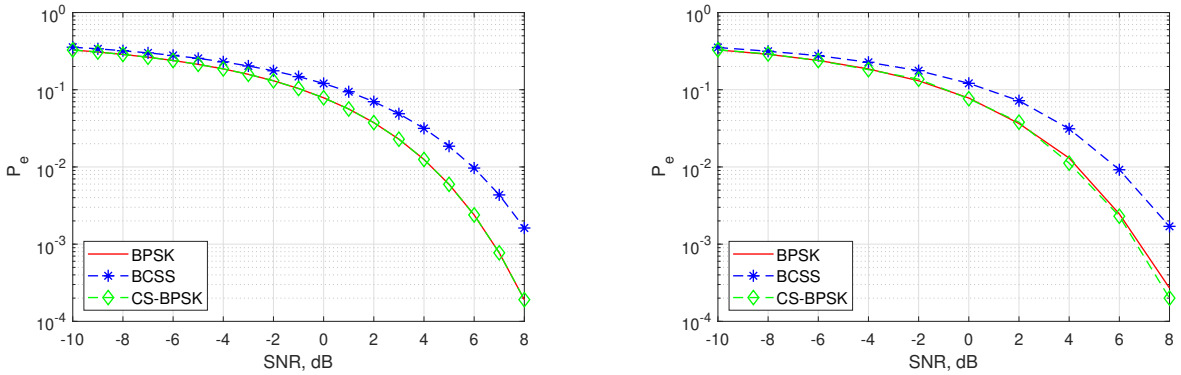

(a) Analytical result (b) Simulation result

Figure 3: Analytical probability of error of BPSK, BCSS and CS-BPSK (left) and simulated (right) probability of error of above mentioned modulation scheme in AWGN channel.

To examine the performance of the aforesaid modulation schemes across the absorption lines of the THz frequencies, we considered 183 GHz, 380 GHz, and 988 GHz for simulation. The modulated IF signals are up-converted to one of the absorption lines to measure the BER performance. Due to the broadening of the absorption lines with distance (as explained in Section 2), different bandwidths are considered for the modulation. At 183 GHz, a bandwidth of 5 GHz is considered for a 250 m wireless communication link and 10 GHz for a 500 m link. Similarly, we consider 5 GHz and 10 GHz bandwidth for 25 m and 50 m wireless links at 380 GHz, respectively. Furthermore, to test the performance close to 1 THz, we consider the 988 GHz absorption line. 5 GHz and 10 GHz bandwidths are utilized for 1 m and 2 m wireless links, respectively. Furthermore, for 5 GHz and 10 GHz systems we consider the data rates as 2.5 Gbps and 5 Gbps respectively. Here, we change the data rate with bandwidth for a fair comparison with the BPSK. Since for BPSK, the data rate is dependent on bandwidth, and for CSS, the data rate is independent of bandwidth. The detailed list of parameters used to conduct the simulation are presented in Table 1.

Table 1: Simulation parameters.

Carrier frequency and bandwidth consideration

Carrier frequency (GHz)	Distance (m)	Bandwidth (GHz)
183	250/500	5/10
380	25/50	5/10
988	1/2	5/10

Other parameters

Parameter	Value
Humidity	40 %
Temperature	293 Kelvin
Pressure	1 atm
Noise consideration	AWGN

In Figure 4, the BER performance of BPSK, BCSS, and CS-BPSK is shown. It is observed that CS-BPSK has the best performance among the three schemes in the case of communication across the absorption peaks. The performance of the BCSS is close to BPSK. For CS-BPSK and BCSS, power is spread over the whole bandwidth, which makes them robust against the frequency selective attenuation across the absorption peaks. However, for BPSK, the maximum power is centered near the carrier frequency, which results in higher attenuation of the signal compared to CSS schemes. Therefore, BPSK show little improvement in terms of BER compared to CS-BPSK and BCSS.

To realize the improvement in BER with the increase in bandwidth for the similar absorption loss at a particular distance, we considered modulation schemes (CS-BPSK, BCSS, and BPSK) with 5 GHz (2.5 Gbps data rate), and 20 GHz bandwidth across the 183 GHz absorption line for a 500 m long communication link. It is seen that (Figure 5), with the increase of bandwidth, CS-BPSK and BCSS have significantly lower BER. However, there is a nominal improvement in the case of BPSK. The results motivate and justify the use of chirp spread modulation schemes, especially CS-BPSK, over BPSK.

5. EXPERIMENTAL SETUP AND RESULTS

In this section, experimental results are provided by comparing BPSK, BCSS, and CS-BPSK modulation schemes. The TeraNova testbed[29] is utilized for the purpose. In view of the fact that the front-ends are designed to operate in the first absorption defined transmission window above 1 THz (1-1.05 THz), the experimental results provide the comparison of the schemes in the band between two absorption peaks.

5.1 TeraNova Testbed

In Figure 6, the TeraNova testbed, and its corresponding block diagrams are described. The testbed is divided into two parts, namely the hardware components and the software-defined physical layer.

In terms of hardware, on the transmitter side, an analog signal generator (PSG, Keysight E8257D) is utilized to generate the Local Oscillator (LO) frequency between 41.67 GHz and 43.75 GHz. A custom-designed Schottky-diode-based chain of frequency multipliers by Virginia Diode Inc. (VDI), is utilized to upconvert the LO to the radio frequency (RF) between 1 THz and 1.05 THz. At the end, a mixer based on the same technology is utilized to mix the modulated intermediate frequency (IF) signal generated by a state-of-the-art Arbitrary Waveform Generator (AWG, Keysight M8196A). The achievable maximum output power is -15 dBm or 30 μW with the current technology available. On the receiver side, a second PSG and a frequency multiplier chain with a mixer based on the similar technology is utilized to down-convert the received RF frequency to the IF band. A state-of-the-art Digital Storage Oscilloscope (DSO, Keysight DSOZ632A) is utilized to digitize, visualize, and store the received signals for further processing.

The software-defined physical layer is used to implement the pre and post signal processing blocks in the software domain using MATLAB for the transmitter and the receiver module, respectively. In the transmitter, the user-provided data bits are encapsulated into frames. The header and the training sequence are added to the data bits to structure the frame. As a header, a 18-bit-long maximal merit factor (MF) sequence, with optimal correlation properties, is utilized to detect the beginning of a new frame. The training sequence (up to 20 % of

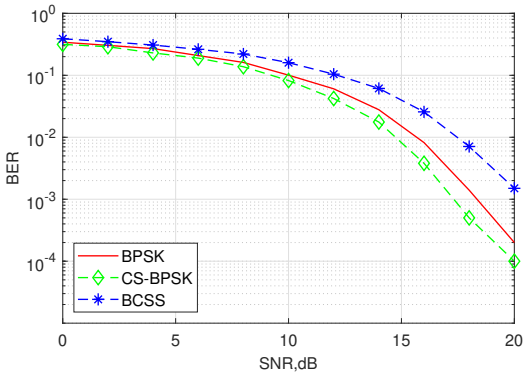

(a) f_c of 183 GHz with 5 GHz BW at 250 m distance

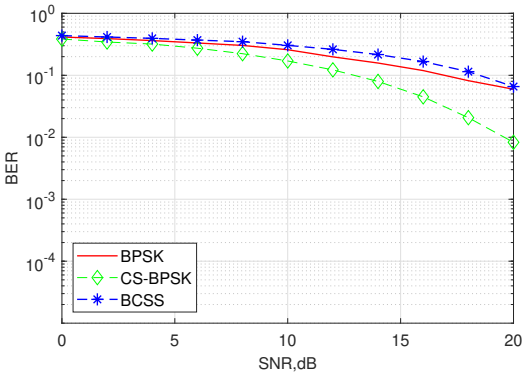

(b) f_c of 183 GHz with 10 GHz BW at 500 m distance

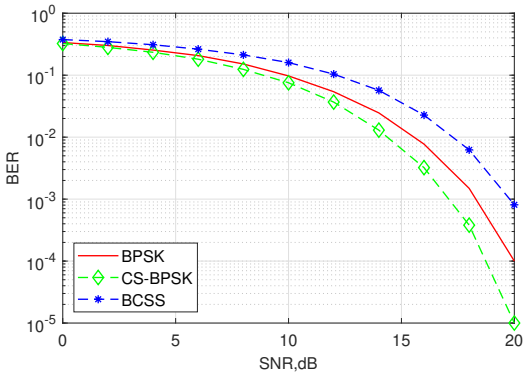

(c) f_c of 380 GHz with 5 GHz BW at 25 m distance

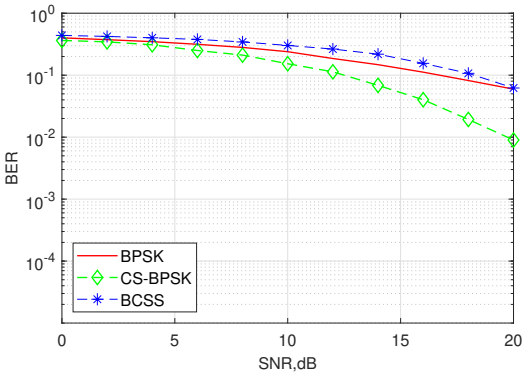

(d) f_c of 380 GHz with 10 GHz BW at 50 m distance

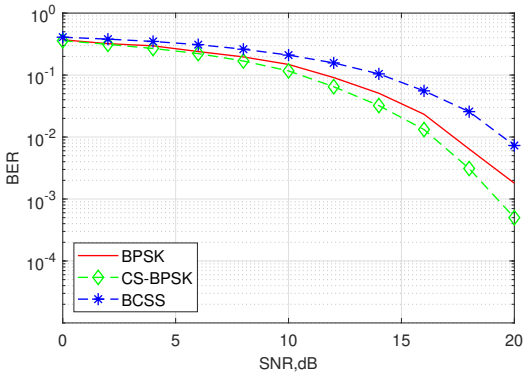

(e) f_c of 988 GHz with 5 GHz BW at 1 m distance

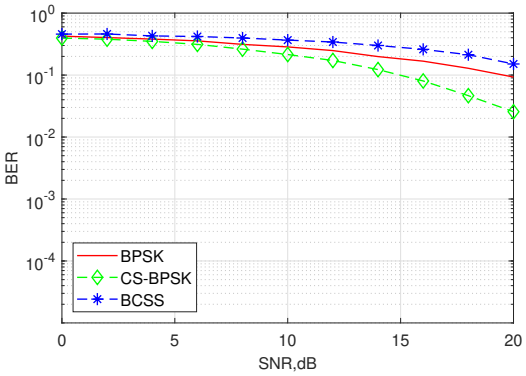

(f) f_c of 988 GHz with 10 GHz BW at 2 m distance

Figure 4: BER for the three modulation schemes under analysis (BPSK, BCSS and CS-BPSK) with different bandwidth (5 GHz and 10 GHz) and over different absorption lines (183 GHz, 380 GHz and 988 GHz) and distances (1 m, 2 m, 25 m, 50 m, 250 m and 500 m).

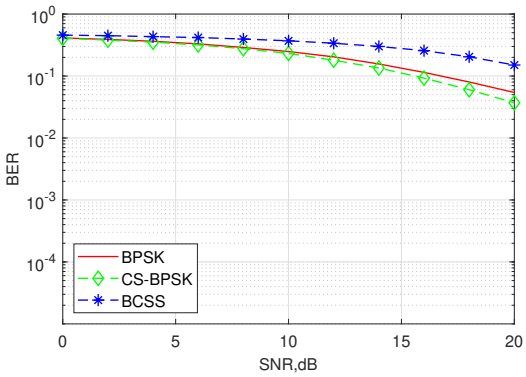

(a) f_c of 183 GHz with 5 GHz BW at 500 m distance

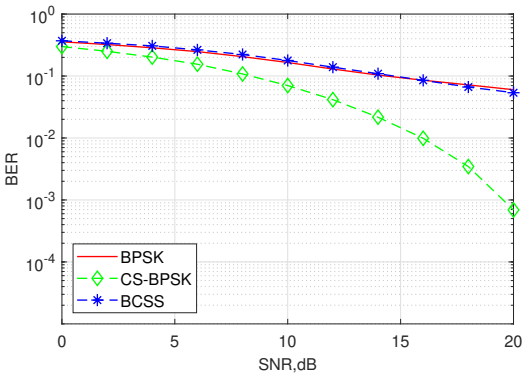

(b) f_c of 183 GHz with 20 GHz BW at 500 m distance

Figure 5: BER performance of BPSK, BCSS, and CS-BPSK across 183 GHz absorption line at the distance of 500 m with the bandwidth of 5 GHz (2.5 Gbps data rate) and 20 GHz (10 Gbps data rate).

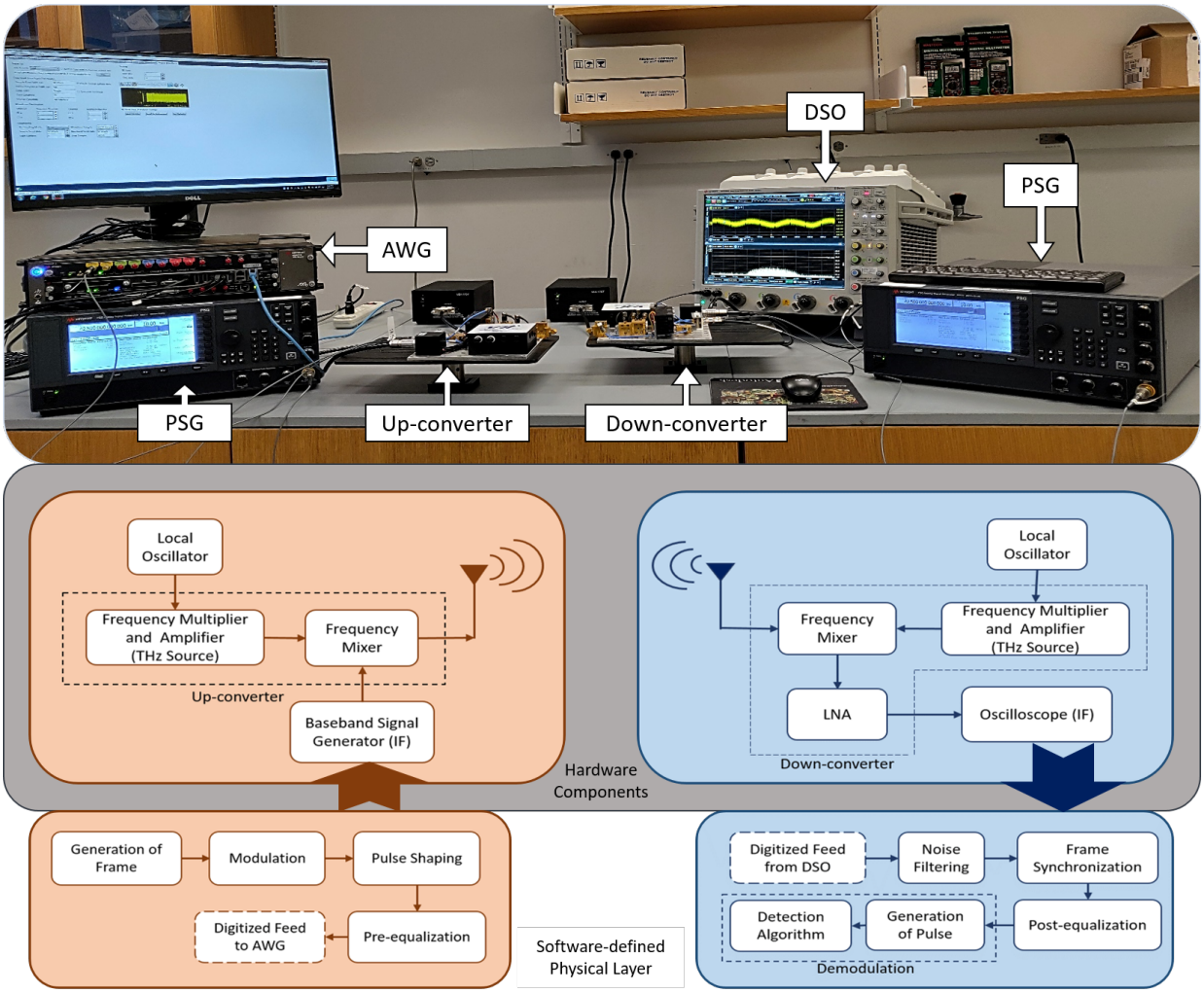

Figure 6: The Teranova testbed (top); schematic diagram of the TeraNova hardware components (middle); and diagram of the software-defined physical layer (bottom) for transceiver system.

data bits) accommodates the bits known to the receiver and is utilized to estimate the channel and equalize the received signal. The generated frames are then passed through the "Modulation" block to modulated the bits according to the different modulation schemes. The "Pulse shaping" block makes use of the raised cosine pulse filter to restrict the signal within the limit of the bandwidth. Furthermore, to compensate constant frequency selective response of the hardware components "Pre-equalization" filter is utilized.

In the receiver, after capturing the IF signal in DSO, the signal is filtered to eliminate band noise from the captured signal. A Chebyshev bandpass filter (based on Parks-McClellan-algorithm) is utilized for the purpose. Subsequently, the frame is synchronized to detect the starting point of the captured signal using the known MF sequence, which is essential for further equalization and correct detection of the bits. Within the "Post-equalization" block, a linear filter equalizer with minimum mean square error (MMSE) statistics is utilized to mitigate the effect of ISI, frequency selective nature of the channel, and path loss. The error between the transmitted training symbols, $\hat{s}$, and output of the post-equalizer, $R\hat{f}$, is minimized to get the filter coefficient vector $\hat{f}$. Where R is the Toeplitz matrix with the received training symbols of dimension. To detect the data bits, the equalized signal are passed through "Demodulation" block. A maximum likelihood (ML) criterion based correlator-type detector is utilized to recover the data bits and given by,

$$\hat{m} = \arg\max_{1 \leq m \leq M} \left(\int_0^T r(t) x_m(t) dt - \frac{1}{2} ||x_m||^2 \right), \tag{11}$$

where $\hat{m}$ denotes the maximum match with a particular symbol and m=1,2,.... M. M is the modulation index. r represents the received symbol. For the purpose of matching, all possible symbols x_m are generated after convolving with raised cosine pulse.

5.2 Experimental Results

In order to check the experimental BER performance of the BPSK, BCSS, and CS-BPSK schemes and compare them at true THz frequencies, the modulated IF signals are up-converted to 1.03 THz. In this case, IF modulated signals of 5 GHz and 10 GHz bandwidth are considered with varying distances up to 30 cm. In Table 2, we summarize the results of different schemes when increasing the communication distance. To calculate the BER, ten-frames are considered (each 1,200 bits long).

It is observable that CS-BPSK has the lowest BER, i.e., the best performance, followed by BPSK and BCSS. It is because of the frequency selective nature of the end-to-end channel due to components (cables, connectors, and front-ends). However, the bandwidth leakage is higher for the CS-BPSK and BCSS modulation schemes, which requires the increased guard band for multi-access communication system design. Unlike BPSK, the bandwidth of the CS-BPSK and BCSS modulation schemes is independent of the symbol duration, which leverages the use of a higher bandwidth signal for better performance in terms of BER. In other words, by increasing the bandwidth and keeping the symbol rate same, we can decrease the BER and create a more robust modulation scheme for the communication across the absorption peaks.

6. CONCLUSION

In this paper, we proposed the CSS scheme for communication across the absorption peaks of the THz Band to overcome the high path-loss and the frequency selectivity of the channel. We studied the performance of CS-BPSK and BCSS both analytically and numerically, in the presence of AWGN flat channel and across the different absorption peaks. The TeraNova testbed is utilized to experimentally demonstrate the BER at various distance. We observed that CS-BPSK outperforms the traditional BCSS and BPSK in terms of BER. Moreover, the bandwidth of the CS-BPSK and BCSS modulation schemes is independent of its symbol duration, which in our case can be leveraged to trade higher bandwidth for lower BER. Hence, the proposed modulation technique sparks interest in reliable long-range communications across the absorption peaks of the THz band. In future, we can extend this work in the direction of multiple-array modulation(i.e, CS-MPSK) and formulate an optimization problem to determine the spread of the bandwidth and data-rate to maintain the required BER.

Table 2: Measured BER for different modulation schemes.

BPSK

BW(GHz)/Bit rate(Gbps)	Distance(cm)	SNR(dB)	BER
5 / 2.5	5	13.4	0
	10	8.7	0
	15	4.5	2.5×10^{-3}
	20	2.5	1×10^{-2}
	25	0.4	7.8×10^{-2}
	30	-0.8	9×10^{-2}
10 / 5	5	11.5	0
	10	6.8	1.6×10^{-3}
	15	2.6	3×10^{-2}
	20	0.8	7×10^{-2}
	25	-0.5	1.7×10^{-1}
	30	-1.9	2.5×10^{-1}

BCSS

BW(GHz)/Bit rate(Gbps)	Distance(cm)	SNR(dB)	BER
5 / 2.5	5	12.5	0
	10	7.7	8.4×10^{-4}
	15	3.9	6×10^{-3}
	20	2.5	2.5×10^{-2}
	25	1.2	9.2×10^{-2}
	30	-0.5	1.2×10^{-1}
10 / 5	5	11	0
	10	6.1	4.1×10^{-3}
	15	3.1	4.4×10^{-2}
	20	1.2	1×10^{-1}
	25	0.2	1.8×10^{-1}
	30	-1.5	2.4×10^{-1}

CS-BPSK

BW(GHz)/Bit rate(Gbps)	Distance(cm)	SNR(dB)	BER
5 / 2.5	5	12.7	0
	10	7.5	0
	15	4.5	1.6×10^{-3}
	20	2.8	1.4×10^{-2}
	25	1.5	5.2×10^{-2}
	30	0.1	8.4×10^{-2}
10 / 5	5	11.7	0
	10	6	0
	15	3.4	1.9×10^{-2}
	20	1.5	4.7×10^{-2}
	25	0.2	1.2×10^{-1}
	30	-1.9	1.6×10^{-1}

Acknowledgements

This work was supported by the U.S. National Science Foundation Grant No. CNS-2011411 and the U.S. AFRL Grant No. FA8750-20-1-0200.

REFERENCES

[1] Forecast, C. V., "Cisco visual networking index: Global mobile data traffic forecast update, 2017–2022 white paper," (2019).

[2] Akyildiz, I. F., Jornet, J. M., and Han, C., "Terahertz band: Next frontier for wireless communications," *Physical Communication* **12**, 16–32 (2014).

[3] Song, H.-J. and Nagatsuma, T., "Present and future of terahertz communications," *IEEE transactions on terahertz science and technology* **1**(1), 256–263 (2011).

[4] Kürner, T. and Priebe, S., "Towards thz communications-status in research, standardization and regulation," *Journal of Infrared, Millimeter, and Terahertz Waves* **35**(1), 53–62 (2014).

[5] Kurita, Y., Ducournau, G., Coquillat, D., Satou, A., Kobayashi, K., Boubanga Tombet, S., Meziani, Y., Popov, V., Knap, W., Suemitsu, T., et al., "Ultrahigh sensitive sub-terahertz detection by inp-based asymmetric dual-grating-gate high-electron-mobility transistors and their broadband characteristics," *Applied Physics Letters* **104**(25), 251114 (2014).

[6] Radisic, V., Leong, K. M., Scott, D. W., Monier, C., Mei, X., Deal, W. R., and Gutierrez-Aitken, A., "Sub-millimeter wave inp technologies and integration techniques," in [*2015 IEEE MTT-S International Microwave Symposium*], 1–4, IEEE (2015).

[7] Mehdi, I., Siles, J. V., Lee, C., and Schlecht, E., "Thz diode technology: status, prospects, and applications," *Proceedings of the IEEE* **105**(6), 990–1007 (2017).

[8] Brown, E., McIntosh, K., Nichols, K., and Dennis, C., "Photomixing up to 3.8 thz in low-temperature-grown gaas," *Applied Physics Letters* **66**(3), 285–287 (1995).

[9] Gobel, T., Schoenherr, D., Sydlo, C., Feiginov, M., Meissner, P., and Hartnagel, H., "Single-sampling-point coherent detection in continuous-wave photomixing terahertz systems," *Electronics Letters* **45**(1), 65–66 (2008).

[10] Preu, S., Döhler, G., Malzer, S., Wang, L., and Gossard, A., "Tunable, continuous-wave terahertz photomixer sources and applications," *Journal of Applied Physics* **109**(6), 4 (2011).

[11] Akyildiz, I. F. and Jornet, J. M., "Graphene-based plasmonic nano-antenna for terahertz band communication," (May 9 2017). US Patent 9,643,841.

[12] Han, C., Jornet, J. M., and Akyildiz, I., "Ultra-massive mimo channel modeling for graphene-enabled terahertz-band communications," in [*2018 IEEE 87th Vehicular Technology Conference (VTC Spring)*], 1–5, IEEE (2018).

[13] Jornet, J. M. and Akyildiz, I. F., "Channel modeling and capacity analysis for electromagnetic wireless nanonetworks in the terahertz band," *IEEE Transactions on Wireless Communications* **10**(10), 3211–3221 (2011).

[14] Jornet, J. M. and Akyildiz, I. F., "Femtosecond-long pulse-based modulation for terahertz band communication in nanonetworks," *IEEE Transactions on Communications* **62**(5), 1742–1754 (2014).

[15] Hossain, Z. and Jornet, J. M., "Hierarchical bandwidth modulation for ultra-broadband terahertz communications," in [*ICC 2019-2019 IEEE International Conference on Communications (ICC)*], 1–7, IEEE (2019).

[16] Han, C. and Akyildiz, I. F., "Distance-aware multi-carrier (damc) modulation in terahertz band communication," in [*2014 IEEE International Conference on Communications (ICC)*], 5461–5467, IEEE (2014).

[17] Kim, J.-H., Younis, M., Moreira, A., and Wiesbeck, W., "A novel ofdm chirp waveform scheme for use of multiple transmitters in sar," *IEEE Geoscience and Remote Sensing Letters* **10**(3), 568–572 (2012).

[18] Wang, W.-Q., "Mimo sar ofdm chirp waveform diversity design with random matrix modulation," *IEEE Transactions on Geoscience and Remote Sensing* **53**(3), 1615–1625 (2014).

[19] Winkler, M., "Chirp signals for communication," *1962.* (1962).

[20] Karapistoli, E., Pavlidou, F.-N., Gragopoulos, I., and Tsetsinas, I., "An overview of the ieee 802.15. 4a standard," *IEEE Communications Magazine* **48**(1), 47–53 (2010).

[21] Wu, L., Trezzo, J., Mirza, D., Roberts, P., Jaffe, J., Wang, Y., and Kastner, R., "Designing an adaptive acoustic modem for underwater sensor networks," *IEEE Embedded Systems Letters* **4**(1), 1–4 (2011).

[22] Demirors, E., Sklivanitis, G., Santagati, G. E., Melodia, T., and Batalama, S. N., "Design of a software-defined underwater acoustic modem with real-time physical layer adaptation capabilities," in [*Proceedings of the International Conference on Underwater Networks & Systems*], 1–8 (2014).

[23] Huang, S.-W. and Pados, D. A., "M-ary orthogonal chirp modulation for coherent and non-coherent underwater acoustic communications," *arXiv preprint arXiv:1803.02950* (2018).

[24] Li, X., Bai, Z., and Kwak, K., "Nbi suppression uwb system based on novel nonlinear chirp pulses," in [*2009 9th International Symposium on Communications and Information Technology*], 1167–1170, IEEE (2009).

[25] Wang, Q., "Non-linear chirp spread spectrum communication systems of binary orthogonal keying mode," (2015).

[26] Gerecht, E., Douglass, K. O., and Plusquellic, D. F., "Chirped-pulse terahertz spectroscopy for broadband trace gas sensing," *Optics express* **19**(9), 8973–8984 (2011).

[27] Yang, X., Pi, Y., Liu, T., and Wang, H., "Three-dimensional imaging of space debris with space-based terahertz radar," *IEEE Sensors Journal* **18**(3), 1063–1072 (2017).

[28] Huang, S.-W., Sklivanitis, G., Pados, D. A., and Batalama, S. N., "Underwater acoustic communications using quasi-orthogonal chirps," in [*2017 51st Asilomar Conference on Signals, Systems, and Computers*], 1749–1753, IEEE (2017).

[29] Sen, P. and Jornet, J. M., "Experimental demonstration of ultra-broadband wireless communications at true terahertz frequencies," in [*2019 IEEE 20th International Workshop on Signal Processing Advances in Wireless Communications (SPAWC)*], 1–5, IEEE (2019).